Interplay between geological materials and the environment at the Dazu Rock Carvings, China

Haiqing Yang [a], Xingyue Li [a*], Francesca Cappitelli [b]

Author affiliations

[a] School of Civil Engineering, Chongqing University, Chongqing, China

[b] Department of Food, Environmental and Nutritional Sciences, Università degli Studi di Milano, via L. Mangiagalli 25, 20133, Milan, Italy

Corresponding authors: Xingyue Li (lixingyue@stu.cqu.edu.cn); ORCID: 0000-0003-1058-5228

First author: Haiqing Yang (yanghaiqing@cqu.edu.cn); ORCID: 0000-0003-4497-044X

Third author: Francesca Cappitelli (francesca.cappitelli@unimi.it); ORCID: 0000-0003-1237-1813

Abstract

The study of the historical built environment is of great significance to the heritage conservation and the reconstruction of the level of anthropogenic pollution in the past. On the Dazu Rock Carvings, China, a black to reddish-brown, relatively dense mineral film with a thickness of approximately 150 μm was observed on the surface of sandstone. The chemical composition of the mineral film studied by SEM-EDS, EPMA, XAS, TOC, and IC, revealed that its development was comprehensively controlled by environmental conditions, especially by environmental pollution. The bacterial community was also investigated by next generation sequencing and its potential metabolisms through PICRUSt2. Overall, it was proved that the mineral film commonly found on the surface of the investigated sandstone and its microbiome provided a certain degree of protection to the internal sandstone structure. Variation in S in the mineral film along the depth direction aligned consistently with the annual cumulative variation trend of SO_2 in the region over the past 20 years. This alignment served as a reliable means to monitor and investigate the concentration changes of SO_2 in the atmosphere. Besides the relevance for stone heritage conservation, this study provides insights into the interplay between geological materials and the environment. (Because of the limitation of *Environmental Science & Technology* on the number of abstract words, some contents are deleted.)

Keywords: mineral film; environmental pollution; potential metabolisms; passive sampler; protective action; next generation sequencing

SYNOPSIS

This paper finds that the mineral film and its microflora on the surface of sandstone have a certain protective effect on the internal structure of sandstone.

Introduction

Material remains of history and cultural heritage possess intangible value because they provide invaluable insights into human civilization[1-3]. However, numerous large stone cultural heritage endures direct exposure to the natural environment, rendering them vulnerable to the erosive forces of weathering[4, 5]. The continual influence of the environment, encompassing climate and atmospheric conditions, gradually degrades these materials. Over time, this detrimental influence inevitably leads to the development of micro-damage, a subtle but cumulative effect that profoundly influences the stability and overall durability of stone cultural heritage[6-9].

Environmental pollution[10-12] and acid rain[13, 14] have significantly accelerated the erosion and damage of stone cultural heritage. Deterioration phenomena are manifested on the surface of stone materials in various forms, such as patina-like depositions, soiling, and crusts varying from a few millimeters to centimeters in thickness. Numerous forms of crusts can be found on the surface of stone materials, ranging in color from gray to black, and appearing layered, framed, or cauliflower-like[15-19]. The chemical composition of these crusts may exhibit significant variations based on a number of factors, such as the inherent characteristics of the materials, the geographical location of the structure/building, and the specific environmental conditions in which the structure/building is situated[20].

The presence of gypsum ($CaSO_4$) can often be detected in crusts on stone surface. The formation of gypsum crusts is related to the presence of SO_2, an atmospheric pollutant. SO_2 can be transferred to the stone surface through dry or wet deposition processes[21, 22]. When in contact with water, SO_2 dissolves to form an acidic solution, which reacts with Ca^{2+} in stone materials to form gypsum. This crust has been found in limestone, calcareous sandstone, and even in sandstone without primary $CaCO_3$[12, 23, 24]. The Ca^{2+} can come from both calcite and the hydrolysis of plagioclase minerals in an acidic environment[9]. Generally, gypsum crusts are more common in areas with severe SO_2 pollution, especially in urban industrial environments[12]. During the growth of the crusts, gypsum crystals capture particulate matter, giving the crust its typical black color[25]. Additionally, particles, containing metals such as Pb, Se, Ni, Cr, and Cu, produced by fossil fuel combustion, mining, and metallurgical activities, can be embedded in the crusts[11, 26, 27].

The weathering crust is often regarded as a passive sampler of atmospheric pollution[11], and some compounds found in the crust can be used as reliable indicators of past environmental pollution. Therefore, cities with varying pollution levels and types have weathering crusts of distinct compositions and structures. Moreover, investigating the elemental composition of weathering crusts over different time periods facilitates the establishment of historical pollution records[27, 28].

Sandstone, a multiphase solid composed mainly of quartz, feldspar and other minerals, possesses high porosity and a complex clastic texture[29, 30]. Gaseous pollutants can easily enter sandstone through its open pore network and interact with its

components[31]. However, during field investigations of various stone relics, it is discovered that despite long-term exposure to natural weathering, biological damage, and acid rain erosion, certain inscriptions on the surface of sandstone remain well-preserved[32]. It has been found that there is a natural coating on the sandstone surface, which can serve as a protective barrier to limit the interaction between the stone and the external medium. To a certain extent, it can reduce the impacts of external weathering mechanisms to sandstone. This is also the reason that sandstone exhibits a decrease in deterioration characteristics in the later stages of weathering. This protecting effect is similar to the one offered by the artificial passivating layers or surface coatings applied on modern industrial materials[33].

Here, we investigated the nature and layers within the weathered crust on the sandstone surfaces of the Dazu Rock Carvings, located in the Dazu District, Chongqing, China (Fig. 1a), that are one of the outstanding representatives of ancient Chinese stone carving art. In particular, we examined the formation processes and response mechanisms of a mineral film discovered within the weathering crust and discussed it in conjunction with its composition and structure. Beyond its impact on heritage conservation, these findings have broader implications for material science, offering insights into the interplay between geological materials and environmental parameters (such as SO_2 emissions).

MATERIALS AND METHODS

Heritage site and sampling. The Dazu Rock Carvings were first created in the Sui Dynasty (581-618 AD), and subsequently underwent construction and expansion during the Tang, Song, Ming, and Qing Dynasties. These carvings have a history of more than a thousand years and are considered to be one of the world's eight major grottoes. In December 1999, the Dazu Rock Carvings, represented by Baodingshan, Beishan, Nanshan, Shimenshan, and Shizhuanshan, were included in the World Heritage List by UNESCO[34]. Among them, the cliff statues on Baodingshan in the Dazu Rock Carvings have the largest scale, the most exquisite craftsmanship, and the highest level of preservation.

The sampling point was mainly located in Dazu Rock Carvings in Chongqing (Fig. 1a). The climate of Dazu area belongs to subtropical warm and humid monsoon climate, with abundant rainfall and distinct seasonal changes. The annual average temperature in this area is 17.2 ℃, the annual average relative humidity is 82.6 %, and the annual average precipitation is 1006.6 mm[14]. The topography of the area where the cliff statues are located is dominated by hills which belong to the Upper Jurassic Penglaizhen Formation (J3p). The lithology is mostly feldspar quartz sandstone.

Sandstone samples were mainly from Baodingshan rock carvings in Dazu, Chongqing. The color of weathered crust layer did not show any obvious difference to the surrounding rock. To verify the existence of mineral film, the samples were tested by various detection methods, including thin section identification, X-ray diffraction (XRD), scanning electron microscopy (SEM), energy dispersive spectrometry (EDS),

electron probe X-ray micro-analysis (EPMA), inductively coupled plasma-optical emission spectrometry (ICP-OES), and synchrotron X-ray absorption spectroscopy (XAS). The list of tested projects and results was shown in supplementary information.

Elemental analysis of the mineral film. SEM-EDS tests were carried out to elucidate the elemental distribution of mineral films in sandstone samples. We used a Tescan Mira4 model scanning electron microscope, with an Oxford Ultim Max65 spectrometer to take SE images and conduct EDS analyses. The working voltage was 15 kv, and the working distance was approximately 14-20 mm.

The organic carbon content of the mineral film was determined using an aj-analyzer (multi N/C 3100). After the pre-acidification of the scraped mineral film powder was completed, the solid sample boat was sent to a high-temperature combustion furnace with a special iron hook for determination.

To determine the distribution patterns of some trace elements in mineral film, a JEOL JXA-8230 electron probe equipped with five spectrometers was used to perform quantitative analysis of elements at different points. Prior to testing, the samples were coated with a uniform carbon film with a thickness of approximately 20 nm[35, 36]. The test conditions were an acceleration voltage of 15 kV, an acceleration current of 20 nA, and a beam spot diameter of 10 μm. All test data were ZAF-corrected. The measurement time for the characteristic peaks of Ti, Cd, Pt, Sr, Ca, Pb, S, W, As, Se, Cu, Fe, Mn, Cr, Ba, and Sb elements was 10 s, and the measurement time for the upper and lower backgrounds was half of the peak measurement time. The reference samples used were as follows: rutile (Ti); cadmium metal (Cd); platinum metal (Pt); celestite (Sr); diopside

(Ca); lead telluride (Pb); indium arsenide (As); pyrite (S); selenium metal (Se); copper metal (Cu); almandine (Fe); rhodonite (Mn); chromium metal (Cr); barite (Ba); and antimony metal (Sb).

Data from 11 test points were obtained on the probe slide, and these points were generally located in a straight line (Fig. 4a). The test results were provided in the Supplementary Information.

Fe K-edge X-ray absorption spectroscopy (XAS) analyses were performed with Si (111) crystal monochromators at the BL14W Beam line at the Shanghai Synchrotron Radiation Facility (SSRF) (Shanghai, China). Before the analysis at the beamline, samples were placed into aluminum sampleholders and sealed using Kapton tape film. The extended X-ray absorption fine structure (EXAFS) spectra were recorded at room temperature using a 4-channel Silicon Drift Detector (SDD) Bruker 5040. Fe K-edge EXAFS spectra were recorded in transmission mode. Negligible changes in the line-shape and peak position of Fe K-edge X-ray absorption near edge structure (XANES) spectra were observed between two scans taken for a specific sample. The EXAFS spectra of these standard samples were recorded in transmission mode. The spectra were processed and analyzed using the software code Athena[37].

Bacterial community analysis. Three samples on the outer surface were obtained by scraping the surface film of the weathering shell with a sterile scalpel. Three inner samples were taken from the inside of the weathering crust. DNA quantification was performed using a Nanodrop. The quality of the extracted DNA was assessed through 1.2% agarose gel electrophoresis. PCR amplification was completed using universal

primers. The primers 338F, 5'ACTCCTACGGGAGGCAG-3', and 806R, 5'-GGACTACHVGGGTWTCTAAT-3', were used to amplify the v3-v4 region[38]. The amplification products were verified using 2% agarose gel electrophoresis, purified with a gel extraction kit (AXYGEN Co., China), and then further analyzed.

The paired-end reads were sequenced from the Illumina MiSeq PE300 platform (Illumina, San Diego, USA) according to the manufacturer 's standard protocol of Majorbio Bio-Pharm Technology Co. Ltd. (Shanghai, China). The original gene readings were multiplexed, filtered for quality by fastp version 0.20.0[39], and merged with the standard standard by FLASH version 1.2.7[40]. Reads shorter than 50 bp, with an average quality score of less than 20 and unclear bases were deleted from the quality data.

UPARSE version 7.1 was used for clustering the clean data into operational taxonomic units (OTUs), with a 97% similarity cutoff[41]. Analysis was performed using the 16S rRNA database (Silva v138) with a confidence threshold of 0.7. Readings that do not match any sequence in the database are clustered into unclassified or normal groups. The community diversity (Shannon index) and richness (Chao index) were calculated using the quantitative insight method of microbial ecology (QIIME) (1.9.0 version).

PICRUSt2 was used to predict the potential function of bacterial communities, and KEGG database was used for functional annotation. Although the function of the microbiome derived from PICRUSt2 should be considered as potential, it can still provide important insights for research.

The sequence data generated in this study have been submitted to NCBI, and the biological project ID is PRJNA1203933.

Analysis of atmospheric data and elemental data. In the study, the source of atmospheric data was the annual environmental status bulletin issued by the Chongqing Municipal Ecological Environment Bureau and the Chongqing Yearbook compiled by the Chongqing Municipal Bureau of Statistics. The correlation analysis of the data was completed in SPSS software.

The porosity of the mineral film and the internal structure were obtained by SEM image processing. Taking the SEM image as the original input image, Fiji image processing software and its built-in plug-in were utilized to count the pores of the sample. The specific analysis steps were as follows: firstly, the defect parts in the image were identified based on a machine learning method (random forest), and the SEM image was binarized. The white area was considered to be the defect part, and the black area was considered to be the sample particle. Secondly, noise processing was carried out on the obtained binary image to filter out the black and white noise in the image. Finally, the pores were statistically calculated by analyzing particles.

The total emissions of SO_2 in the past 20 years could be inferred from the change curve, showing obvious stages in annual emissions where a turning point occurs every few years. The SO_2 emissions over the past 20 years could be divided into five stages: 2002-2005; 2006-2010; 2011-2015; 2016-2018; and 2019-2022. The cumulative emissions of these five stages could be obtained by summing the SO_2 emissions of each stage. Correlation was then performed with the S element data from the first five testing

points in the mineral film.

The data from 11 test points show that the element Cu appeared alternately with a distinct partitioning phenomenon. Cu was often used as an indicator of pollution in research evaluating the impact of climate change on rivers[42-44].

The depth range for each region was calculated. Since only the element data at different points on the vertical weathering crust line were measured in the experiment, the element distribution in the whole region could not be accurately described. Therefore, it was necessary to divide these 11 testing points into different regions. By considering the distribution of the Cu element, a boundary was identified between the two consecutive testing points as the upper or lower interface of this layer. This interface was equal to the two neighboring testing points. The distance d from the interface to the outer edge of the sandstone could be calculated using the following formula:

$$d = u_n + \frac{u_{n+1} - u_n}{2} \quad (1)$$

where u_n and u_{n+1} represent the distance from the outer edge of the sandstone to test point n and test point $n+1$, respectively.

At the same time, according to the location, the 11 test points could be divided into three regions. The first five test points were located in the mineral film zone, the middle four test points were located in the internal cement, and the last two test points were located in a mixed infiltration zone, which connected the bulk and the outside biofilm.

RESULTS AND DISCUSSION

A natural mineral film on the surface of sandstone. Despite long-term outdoor exposure, most of the carvings and surface texts of the Dazu Rock Carvings remained well-preserved. By naked eye, the outer surface of the sandstone revealed a pronounced scaly peeling layer with a reddish-brown appearance (Supplementary Fig. 1).

Sandstone samples were collected in the exposed part of the Dazu Rock Carvings (Fig. 1b). Numerous spherical particles were observed by scanning electron microscopy (SEM) on the outer part of the weathering crust (Fig. 1c). SEM combined with energy-dispersive X-ray spectroscopy (EDS) analysis revealed that the spherical features on this outer layer of the weathering crust were deposited $BaSO_4$, and also microorganisms were likely to be present (Figs. 1d-1e).

The samples taken from Dazu Rock Carvings in Chongqing were processed into longitudinal slices along the direction perpendicular to the surface of the weathering crust. Vertically polished thin sections were observed under a polarizing microscope to elucidate the mineral composition of the sandstone from the inside to the outside (Fig. 2a and Supplementary Fig. 2). The outermost layer of the weathering crust (called 'mineral layer') was a continuous layer, ranging in color from black to reddish-brown, displaying variable morphology and approximately 150 μm thick (Fig. 2a).

To determine whether there was a difference between the mineral layer and the internal part of the weathering crust (internal cement), elemental analysis was performed (Supplementary Table 1). In comparison to the internal cement, the mineral layer exhibited a substantial higher Si content, a significant lower C content, and a moderate higher content of Al, Fe, and K. The contents of Si, Al, Fe and K in the mineral

layer are 8.1 %, 3.2 %, 2.6 % and 2.0 % higher than those in the internal cement, respectively. On the contrary, the C content is 19.9 %, which is lower than 36.5 % of the internal cement.

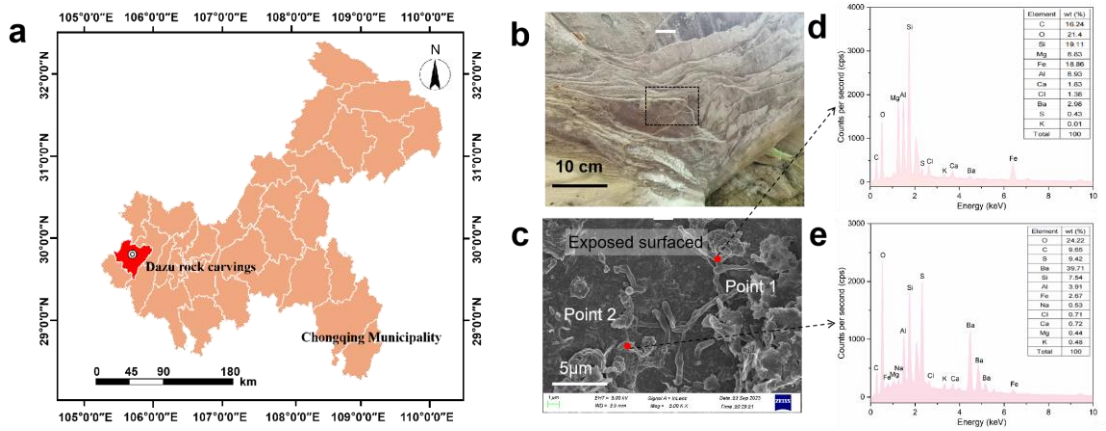

Fig. 1. Morphology of the exposed surface at different scales. a, location of the Daza rock carvings in the Chongqing Municipality. **b,** Top view image of sandstone, the rectangular area is where a sample was taken. **c,** SEM image showing microscopic morphology of the exposed surface of sandstone (5000x). **d-e,** EDS analyses of sandstone point 1 and point 2 of the same sample.

The mineral layer was much denser than the internal cement (Supplementary Fig. 3). The calculated porosity of the mineral film was 3.30%, which was much lower than the 12.57% porosity of the internal structure. Moreover, the mineral layer covering the surface of sandstone was mainly lamellar (Fig. 2b).

In addition, the mineral layer was examined in detail using SEM and EDS in combination with XRD (Supplementary Fig. 4). The mineral layer was made of microscopic quartz (SiO_2), feldspar ($NaAlSi_3O_8$, $KAlSi_3O_8$) particles and clay mineral

aggregates (Fig. 2b). The mineral layer that developed on the surface of the sandstone exhibited a distinctive elemental composition, notably Si, O, Al, Mg, and Fe were present (Fig. 2c). The composition of the mineral layer is also complex, primarily comprising clay minerals including illite ($K(Al,Mg,Fe)_2(Si,Al)_4O_{10}[(OH)_2,(H_2O)]$), kaolinite ($Al_2Si_2O_5(OH)_4$), and chlorite [$(Mg,Fe)_5Al(Si_3Al)O_{10}(OH)_8$], and hematite ($Fe_2O_3$).

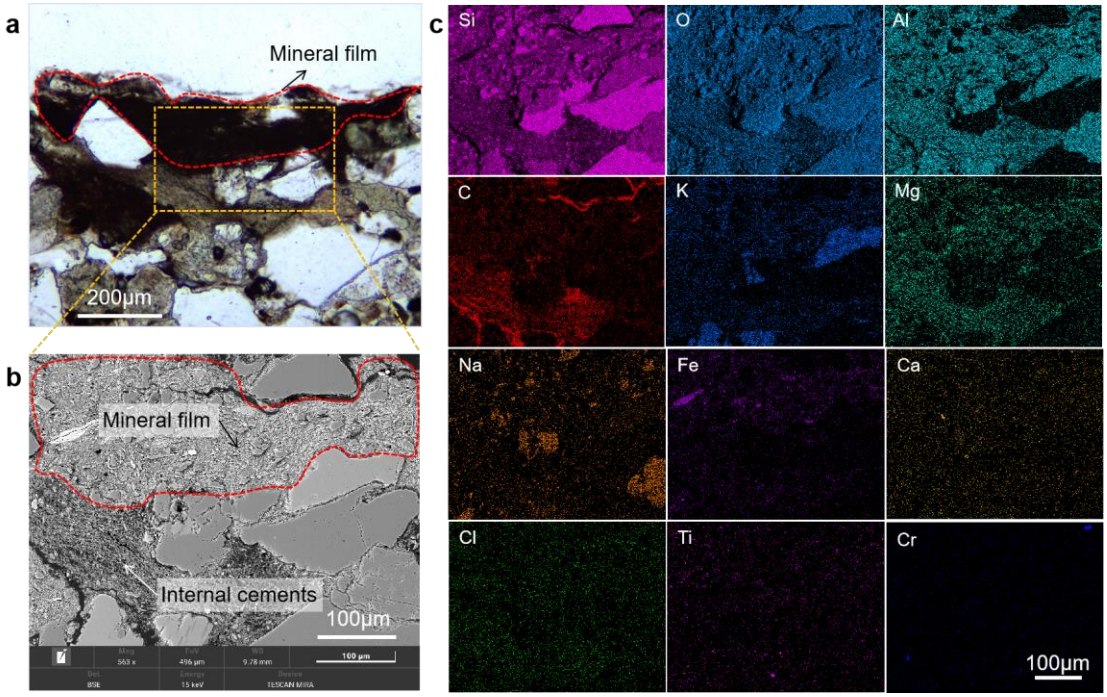

Fig. 2. Morphological and element characteristics of sandstone thin sections. a, Characteristics under polarizing microscope of sandstone weathering crust developed on the Dazu stone outcrop. **b,** Backscattered electron images map of the morphology of the mineral film (the yellow rectangular box in Fig. 2a), showing a relatively dense texture. **c,** SEM-EDS mapping shows the Si, O, Al, C, K, Mg, Na, Fe, Ca, Cl, Ti, and Cr distribution in the sandstone mineral film.

The local structure of Fe in the mineral layer was further studied by the X-ray absorption near edge structure (XANES) measurement at the Fe K edges. Since the K-edge of the same valence Fe ions was not sensitive to the coordination environment, the mineral layer samples could be analyzed using standard reference materials containing different valence Fe ions[45]. We noticed that the K-edge spectrum of the mineral phase does not match that of known Fe_2O_3. It is generally believed that Fe_2O_3 is present on the rock surface due to weathering. However, in our study, its spectrum more closely resembles FeO. The XANES results were further processed by wavelet transform (WT) to visually display the dispersion of Fe, thereby providing radial distance resolution in k and R spaces[46] (Figs. 3c-3f) The XANES results (Supplementary Fig. 5 and Supplementary Table 2) show that the R value of Fe-O in the sample is 2.18 ± 0.01 Å, and the R value of Fe-Fe is 3.07 ± 0.01 Å. This evidence also indicates that FeO, rather than Fe_2O_3, is present in the mineral layer sample. This may be due to acid rain or pollutant gases (such as sulfides and sulfites) promoting the presence of Fe in the form of Fe^{2+} in the surface layer of the sandstone, leading to the formation of FeO.

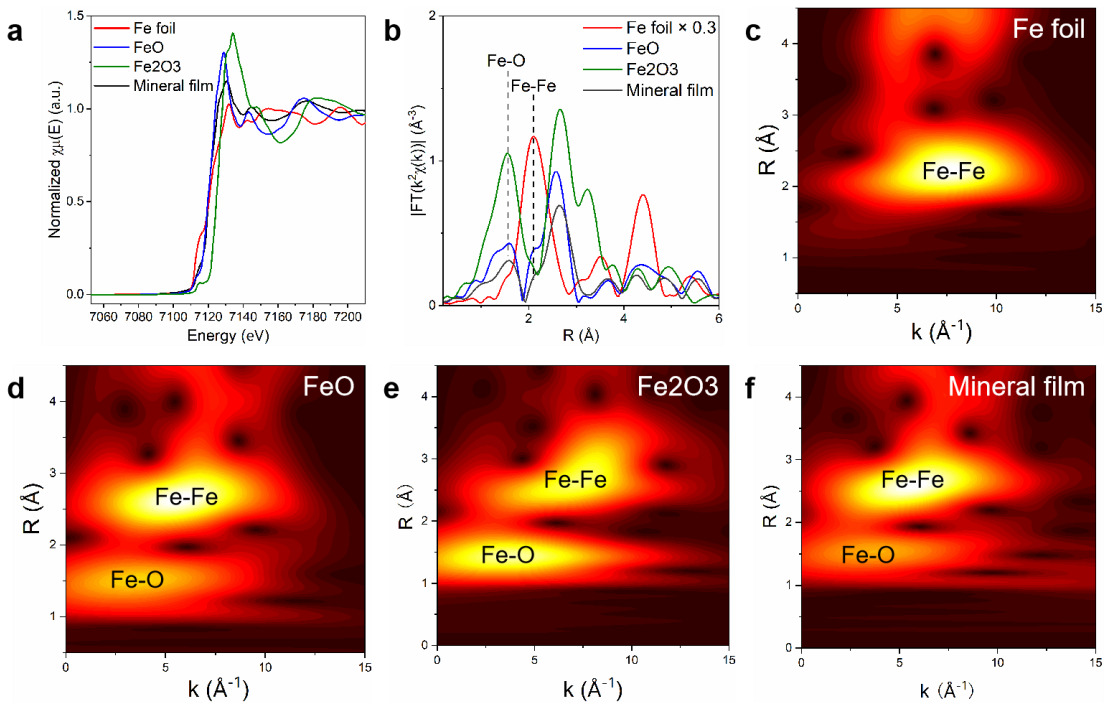

Fig. 3. Fe K-edge X-ray absorption near-edge structure (XANES) spectra of mineral layers. a, XANES spectra. **b,** Radial structure functions. **c-f,** Wavelet transform for Fe foil, FeO, Fe_2O_3, and mineral film. Fe foil, FeO and Fe_2O_3 were used as reference materials the measurements.

After acidification of the mineral film sample, the organic carbon content of the mineral layer obtained was 195.6 mg/kg (TOC analysis, Supplementary Fig. 6). The reason why the content of cement C in the weathering crust is higher than that in the mineral layer might be that the internal environment is more stable. On the contrary, the mineral layer is more vulnerable to the erosion of the natural environment such as acid rain[13]. Microbial colonization and its metabolic products could be a source of organic matter on the surface of the sandstone. In addition, oxalate ions were detected in the samples of the mineral film by ion chromatograph (Supplementary Table 3). As the source of this organic matter may be produced by the microbiome colonizing the

surface, the analysis of the bacterial community was performed.

Analysis of the bacterial community. To investigate the spatial distribution of bacteria on sandstone surfaces under the influence of the mineral layer, high-throughput sequencing of the 16S rRNA gene was performed on three samples from the internal cement and three samples from the mineral film. Actinobacteria was the most abundant phylum level in the sandstone. Its relative abundance in the internal cement was 17.18 % higher than that of the mineral layer (Fig. 4a). On the contrary, the relative abundances of Proteobacteria and Cyanobacteria in the mineral layer were 20.85 % and 8.32 %, respectively, which were higher than those in the internal cement (12.32 % and 2.72 %, respectively). Specifically, a total of 2,559 operational taxonomic units (OTUs) were identified, of which 24.1% were shared between the two layers (Fig. 4b). Each layer contained a number of unique bacteria, although the mineral layer has more unique OTUs than the internal cement. This is consistent with the alpha diversity index derived from amplicon data, indicating that microbial alpha diversity was higher in the mineral layer than in the internal cement (Fig. 4c). The Shannon indexes of the mineral layer and internal cement were 5.43 and 4.81, respectively. In addition, PICRUSt2 was used to predict the potential functions of internal cement and mineral layer bacterial community. The results showed that the relative abundance of denitrification-related genes (*nirK*, *nirS*, *norBC*, and *nosZ*) in the mineral layer was higher than that in the internal cement (Fig. 4d). The total abundance of these genes and the mineral layer are 24 % higher than the internal cement.

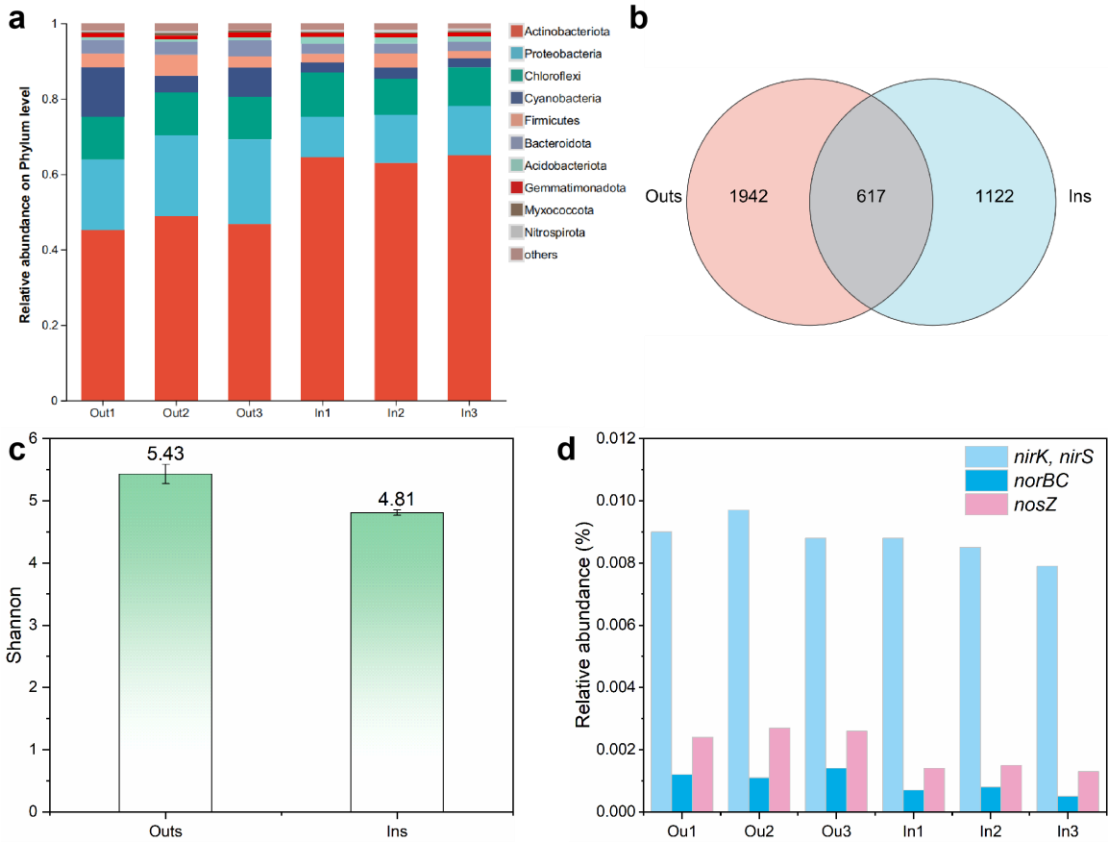

Fig. 4. Composition and diversity of bacterial community. a, Microbial communities in different layers at the phylum level. **b,** The number of shared and unique OTUs between the mineral and the internal cement. **c,** Shannon index of microbial α diversity at different layers. **d,** The relative abundance of genes related to denitrification in different layers. Out: mineral layer, In: internal cement.

A recorder of past pollution. Since ancient times, human activities altered the natural geochemistry of several trace elements. Dust could serve as a carrier for various mixtures of trace metals and metalloids. These trace metal elements were deposited in mineral layers by wind. It was found that the outer layer of the weathering crust is a continuous layer, so it can be called 'mineral film'. The pollution status at the time of deposition could be studied by examining the variations in trace elemental

concentrations at different depths.

Pearson's correlation (R) analysis was carried out to elucidate potential sources of different elements (Supplementary Fig. 7). Fe was a strongly correlated with Cr, W, and Se ($R > 0.67$), indicating that a certain iron oxides might have adsorbed other elements, or Fe might have been co-adsorbed with Cr, W, and Se. At the same time, Mn and Ti had a remarkable association, indicating that they might have originated from the same source. The lack of obvious correlation between Pb, Se, Cu, and Mn confirmed that these metals do not share a common source and transport mechanism.

Variations in the concentration signatures of Pb, Se, Mn, and Cu were analyzed in detail (Fig. 5), given their widely acknowledged association with human activities.

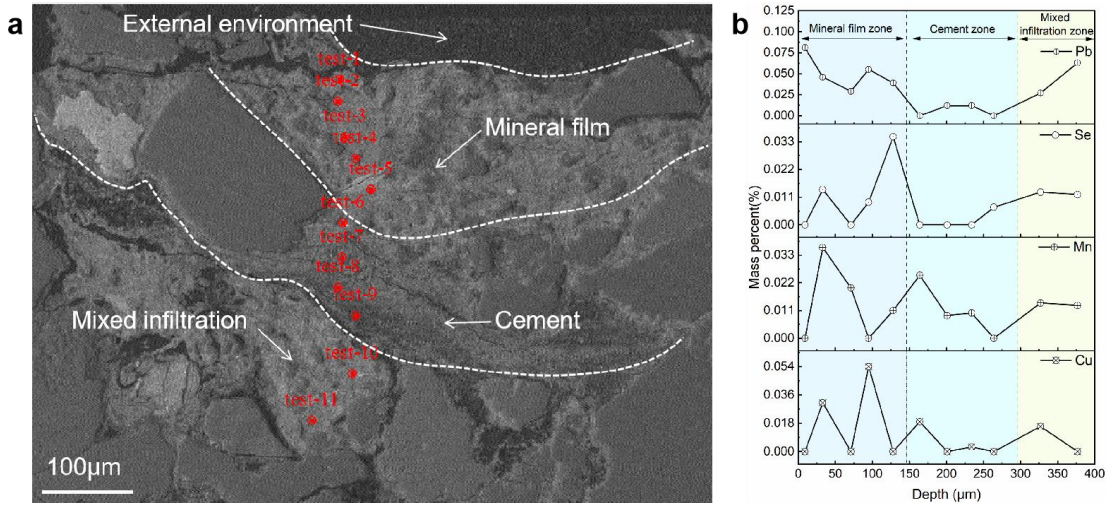

Fig. 5. Electron probe X-ray micro-analyzer (EPMA) tests of the weathering crust. **a,** Probe point schematic diagram, the test points were essentially located on a straight line: the first five test points are located in the mineral film zone, the middle four test points are located in the internal cement, and the last two test points are located in a mixed infiltration zone. **b,** The mass percents of Pb, Se, Mn, and Cu in the mineral,

cement and mixed infiltration zones.

For Pb, the mass fraction of Pb in the mineral film showed a decreasing trend from outside to inside. In addition, the Pb content of the internal cement was significantly lower than that of the other two regions. This confirmed that there was a strong relationship between the change of element content in the mineral film area and the change of external environment. Se exhibited a prominent peak in the mineral film, followed by a substantial decreased in Se content, with data from three test points in the internal cement dropping below the detection limit.

The test results indicated that Cu appeared alternately with a distinct partitioning phenomenon. The content of Cu in the mineral film and the mixed area was also higher than that of the cement. In addition, the Cu and Mn content in the mineral film and mixed zone (zone closer to the inside than the cement zone but connected to the outside on the other side) was greater than in the internal cement. In the internal cement, the elemental content decreased with increasing distance from the surface. At the two test points in the mixed zone (Fig. 5b), the contents of these elements increased again, which indicated that the clay-enriched matrix would block the penetration of ions. This reflected the deposition of dust particles on the original surface of sandstone. Therefore, the mineral film could effectively prevent some metallic elements from infiltrating into the sandstone.

S in the mineral film generally originated from atmospheric SO_2. Fig. 6 aims to explore the relationship between S element variation in the mineral film and SO_2

emissions. The emissions of SO_2 in the past 20 years had exhibited significant changes in five stages. Comparing the cumulative SO_2 emissions in these five stages with the S content in the first five layers of the mineral film, it was found that the trends between the two are consistent, suggesting that atmospheric SO_2 pollutants were likely to be one of the main factors causing changes in S content in the mineral film.

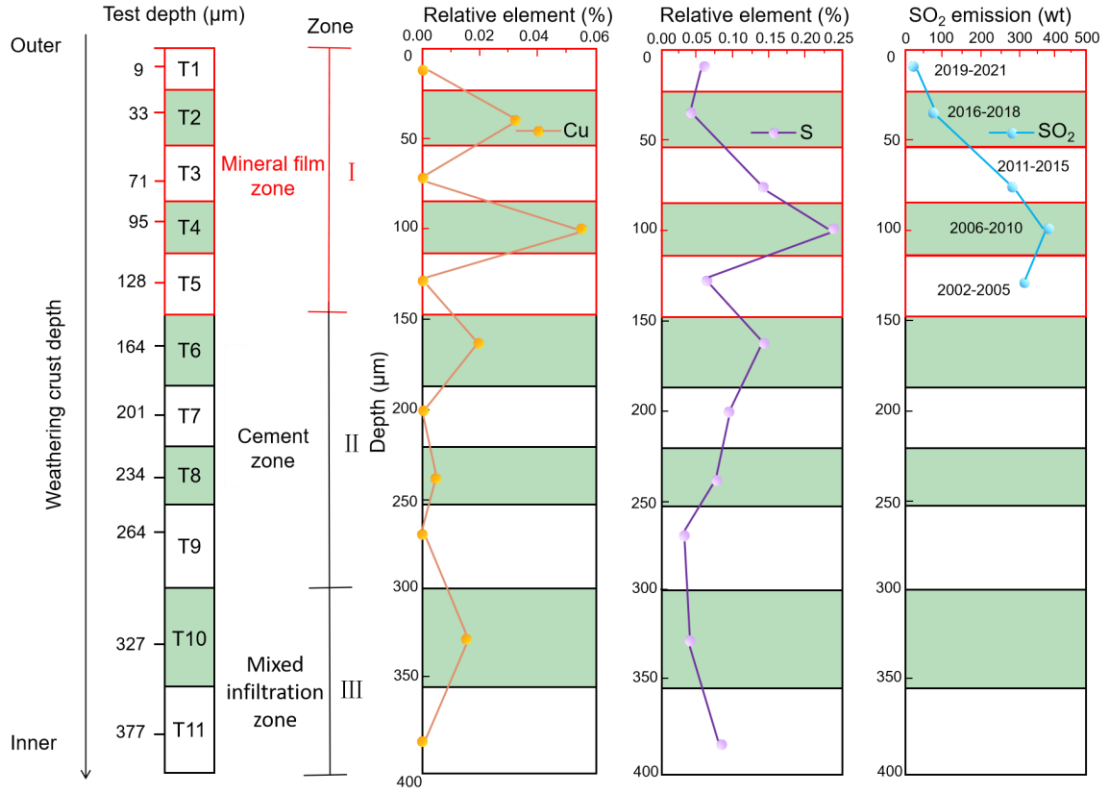

Fig. 6. The relationship between SO_2 emissions and S element content. According to the test points, the weathering crust is divided into 11 test zones (T1-T11). The mass fraction of S as a function of depth and SO_2 emissions in different time periods is shown.

Formation process and protective mechanisms of the mineral film.

The formation of sandstone mineral film was the result of the action of dust deposition, pollutant adsorption and microbial activity under ambient conditions. In the mineral

film, some elements related to human activities were detected. Among them, the metal Ba could be emitted into the atmosphere as particulate matter from road traffic, though it might have also accumulated due to microbial activity[47-50]. Pb in the mineral film mainly came from the use of Pb-containing gasoline[28, 51, 52]. In fact, it was banned in most jurisdictions decades ago due to the markedly deleterious effects of lead on the environment and human health. China also completely stopped producing and selling leaded gasoline in 2000[53]. Prior to the ban, however, the length of time of usage of Pb-containing gasoline was sufficient to cause a large amount of Pb to be released into the atmosphere. Se was mainly derived from the use of coal[54]. China was one of the largest energy-consuming countries in the world, with coal accounting for nearly 60% of its energy consumption[55]. It could be reasonably speculated that the formation of mineral film was related to the soot produced by thermal power generation. Cu in the mineral film could come from industrial emissions, as well as road dust and vehicle emissions[56]. Mn primarily came from the emissions of human and natural activities[54], including automobile exhaust, industrial waste gas, and coal-fired power plant emissions. The increase in the content of Al and K was also the consequence of weathering[14].

The surface structure of sandstone minerals may undergo a series of changes, including physical degradation, chemical reactions, some of which due to microorganisms[57]. In this study, the physical changes included changes in surface flatness and porosity[5]. Chemical reactions involved both dissolution and precipitation of stable phases on the surface of minerals. These reactions would alter the original chemical properties of the mineral surface and reduce the erosion of sandstone by

external factors. The microbiological process refers to the reaction of some bacteria in the mineral film with pollutants or soluble salts in the environment, which enhances the ability of the mineral film to protect cultural heritage.

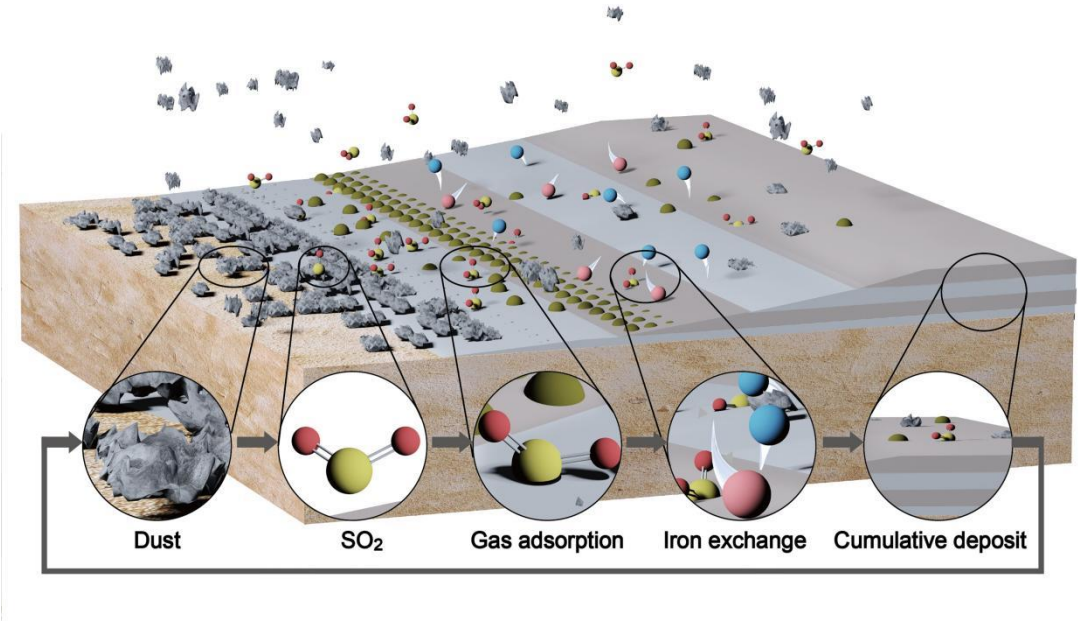

Fig. 7. Hypothesized **formation process of the sandstone mineral film. Step 1:** continuous deposition of dust particles; **Step 2:** adsorption of acidic gases; **Step 3:** ion exchange; **Step 4:** the cumulative deposit of different periods.

In the formation process of mineral film, the first step is adsorption on the surface of sandstone (Fig. 7). The sandstone surface is rough, with the roughness mainly depending on the grain size[7]. When dust in the atmosphere settles on the sandstone due to wind action, the outer surface imparts a good adsorption effect on these particles. Dust deposits typically consist of minerals and soot, containing numerous clay particles and metal elements[58]. These clay particles and some microorganisms in the air will

deposit on the sandstone surface, e.g., through the wind. When the micro-environment of the rock surface (e.g., temperature, humidity, pH, etc.) is suitable for their growth, these microorganisms generate and reproduce[59]. After a prolonged period of cumulative action, clay particles and quartz particles continue to deposit on the sandstone surface, forming the prototype of mineral film.

Next, the contaminants adsorbed on the surface will dissolve. Microorganisms secrete acids able to dissolve rock and mineral dust that contribute to obtain the required mineral ions, such as Ba^{2+} or Ca^{2+}. Most of the anions necessary for the formation of these minerals are related to the effects of air pollutants. For example, sulfate is due to the presence of SO_2, which is a common component of air pollutants. SO_2 can also be adsorbed onto fly ash particles composed of Al, Si, and Fe^{3+}. Moreover, SO_2 could undergo catalysis by Fe^{3+} to generate SO_3 [60]. Given the humid and rainy climate in Chongqing, the produced SO_3 further reacts with water to form SO_4^{2-}. Any unreacted cations react with the generated acid ions or directly with SO_x and NO_x in the air to form some salts, such as barium sulfate[13] (Fig. 1c). These new salts fill the micro-pores of the surface mineral layer making it denser. This action effectively prevents additional foreign pollutants or acid gases from entering the sandstone, which imparts a protective effect.

The existence of a mineral film made sandstone allows resisting external adverse environmental factors. These protection mechanisms could be divided into four parts: physical barrier, microbial protection, adsorption and transformation, and adaptive resistance to pollutants, as shown in Fig. 8.

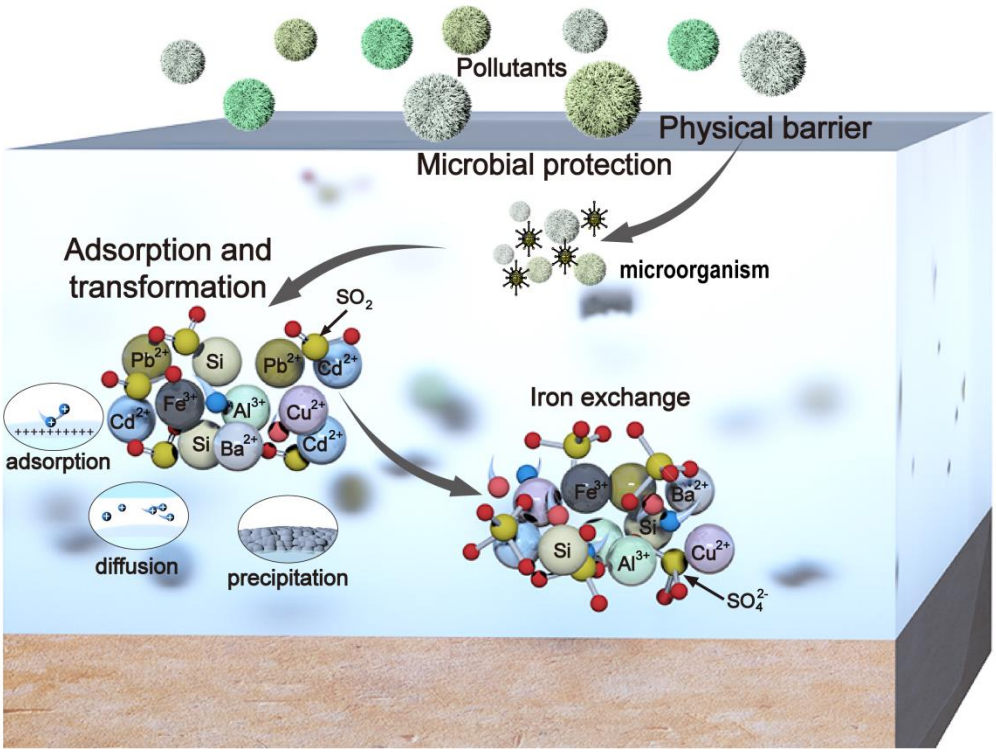

Fig. 8. Proposed protection mechanisms of the sandstone mineral film. The proposed protection mechanisms include physical barriers, microbial protection, adsorption and transformation, and adaptive resistance.

As a physical barrier, mineral film could effectively reduce the penetration of external pollutants, and the their further erosion. During the formation of the mineral film, particles filled the pores of the sandstone, and with continued deposition, the mineral film would become denser. The clay matrices could effectively prevente some metallic elements (Pb, Se, Mn, and Cu) from infiltrating into the sandstone providing protection.

Furthermore, microorganisms carried by the wind during and after the formation of the mineral film could also assist the sandstone in removing pollutants by reaction[61].

The high percentage of Actinobacteria could be explained by their adaptability and resistance to antimicrobials such as heavy metals[62, 63]. In addition, the relative abundance of denitrification-related genes (*nirK*, *nirS*, *norBC*, and *nosZ*) in the mineral layer was higher than that in the inner layer showing that the mineral film has a stronger protective effect and can inhibit weathering by NOx. Moreover, oxalic acid secreted by microorganisms could react with calcium ions to produce calcium oxalate that could block the entry of many substances that cause rock weathering and degradation[64].

The mineral film itself, composed in part clay minerals, acted as an effective natural sorbent that was capable of adsorbing heavy metal ions, such as Pb, Cu, Cd, and Zn[65, 66]. The adsorption of heavy metals on the mineral membrane could be divided into physical adsorption (such as electrostatic adsorption and intraparticle diffusion) and chemical adsorption (such as ion exchange, chemical precipitation, and surface precipitation)[67]. Clay particles generally carry a negative charge. Positively-charged cations could be adsorbed onto the surface of soil particles due to electrostatic attraction[68]. These cations diffused into the pores under the action of a concentration gradient. Ion exchange was the process in which adsorbed ions were replaced by cations in the solution[69]. Precipitation, on the other hand, referred to the process in which free-moving cations in aqueous solution were converted into a solid and deposited on the surface of clay particles under specific pH conditions or when clay minerals contained certain substances, such as carbonates and sulfates[70]. Both of these processes were inherent mechanisms by which mineral films immobilize contaminants.

The microenvironment of the mineral film constituted another line of defense for

protection, encompassing factors such as moisture and the pH value[14] within the sandstone pores. Some minerals in sandstone could be dissolved to form stable new phases to cope with external environmental pollution. Additionally, sandstone could adapt to the erosion of pollutants by adjusting the conditions of the internal environment, especially by buffering pH value[71]. The mineral film would gradually adjust its structure and composition based on the characteristics and concentration of external pollutants.

A natural passive sampler. The studied area, situated in Chongqing, was one of the most polluted regions in China, and coped with elevated levels of gas and particulate matter pollution. In the earlier stages of large-scale industrialization (before 1978), China enjoyed good air quality. However, as economic development surged and urbanization advanced rapidly, the widespread use of traditional energy sources, such as oil and coal, coupled with substantial emissions from industrial waste gases and motor vehicle exhaust, had led to a progressive escalation of environmental pollution. According to statistical data from the Chongqing Yearbook, the total annual emission of SO_2 reached 71.08 million tons in 2006, which constituted the peak of SO_2 emission in the past 20 years. Chongqing was also one of China's important industrial cities, with a predominantly mountainous terrain. The mountainous terrain contributed to the delayed dispersion of pollutants within the city[72]. Furthermore, there was a higher frequency of acid rain in Chongqing.

SO_2 was a gas related to combustion processes[13], primarily generated by the

combustion of fossil fuels and industrial activities. During the formation of mineral film, dust particles adsorbed S-containing aerosols[60]. These molecules would deposit on the surface of rocks through processes such as air movement and particle settling, forming a mineral film. Consequently, changes in the concentration of SO_2 in the air directly impacted the S elemental content in the mineral film.

Emissions of SO_2 had a trend of initially increasing and then decreased over time, with a significant decrease in SO_2 emissions post-2006. Indeed, this indicated that the environmental protection efforts during the 11th Five-Year Plan period had started to produce results. The abnormal S content at sampling point 1 was attributable to its location at a shallower level, making this area more susceptible to the deposition of pollutants, such as SO_2, from the atmosphere, resulting in higher S content. Variation in S in the mineral film along the depth direction aligned consistently with the annual cumulative variation trend of SO_2. This alignment served as a reliable means to monitor and investigate the concentration changes of SO_2 in the atmosphere, facilitating the interpretation of past air quality and environmental pollution. Consequently, the mineral film could be considered to be a natural passive sampler. These mineral films could provide a historical record of the air pollution levels of ambient particulate matter from the moment they begin to grow. The main advantage of using sandstone weathering crust mineral films as passive samplers is that they can provide useful information on the nature and accumulation of metals and polluting gases emitted from the surrounding atmosphere from different anthropogenic and natural sources at no cost.

ASSOCIATED CONTENT

Supporting Information

(Table S1) EDS energy spectrum data of Dazu Rock Carvings sandstone; (Table S2) Structural parameters of different samples extracted from the EXAFS fitting; (Table S3) Concentration of $C_2O_4^{2-}$ in the mineral film; (Fig. S1) Morphology of the collected samples; (Fig. S2) Polarized images of three of the samples; (Fig. S3) Cumulative porosity of internal structure and mineral film; (Fig. S4) Mineral composition of Dazu Rock Carving Sandstone; (Fig. S5) Superimposed curves of experimental results for the samples of mineral film compared with different standard compounds; (Fig. S6) Organic carbon content of mineral film; (Fig. S7) Pearson correlation coefficients among selected elemental attributes.

AUTHOR INFORMATION

Corresponding author

Xingyue Li - School of Civil Engineering, Chongqing University, P R China, 400045;

ORCID: 0000-0003-1058-5228;

Email: lixingyue@stu.cqu.edu.cn

Authors

Haiqing Yang - School of Civil Engineering, Chongqing University, P R China, 400045;

ORCID: 0000-0003-4497-044X;

Francesca Cappitelli - Department of Food, Environmental and Nutritional Sciences, Università degli Studi di Milano, via L. Mangiagalli 25, 20133, Milan, Italy; ORCID: 0000-0003-1237-1813

Author contributions

Haiqing Yang conceived and directed the project; **Xingyue Li** analyzed the experimental results and wrote the manuscript. **Xingyue Li** and **Haiqing Yang** performed the visualisation. **Francesca Cappitelli** discussed the results and commented on the manuscript.

Notes

The authors declare no conflict of interest.

ACKNOWLEDGEMENTS

This work was supported by National Natural Science Foundation of China (No. 52179096) and Chongqing Talent Program Young Top Talents (No. cstc2024ycjh-bgzxm0047).

References

(1) Jroundi, F.; Schiro, M.; Ruiz-Agudo, E.; Elert, K.; Martin-Sanchez, I.; Gonzalez-Munoz, M. T.; Rodriguez-Navarro, C. Protection and consolidation of stone heritage by self-inoculation with indigenous carbonatogenic bacterial communities. *Nat. Commun.* **2017**, *8* (1), 279.

(2) Gu, Z.; Luo, X.; Meng, X.; Wang, Z.; Ma, T.; Yu, C.; Rong, B.; Li, K.; Li, W.; Tan, Y. Primitive Environment Control for Preservation of Pit Relics in Archeology Museums of China. *Environ. Sci. Technol.* **2013**, *47* (3), 1504-1509.

(3) Reimann, L.; Vafeidis, A. T.; Brown, S.; Hinkel, J.; Tol, R. S. J. Mediterranean UNESCO World Heritage at risk from coastal flooding and erosion due to sea-level rise. *Nat. Commun.* **2018**, *9* (1), 4161.

(4) Li, X.; Yang, H.; Chen, C.; Zhao, G.; Ni, J. Deterioration identification of stone cultural heritage based on hyperspectral image texture features. *J. Cult. Herit.* **2024**, *69*, 57-66.

(5) Sun, B.; Li, X.; Cui, K.; Hong, J.; Chen, R.; Jia, C.; Peng, N. Experimental study on the effects of hydrochemistry and periodic changes in temperature and humidity on sandstone weathering in the Longshan Grottoes. *Herit. Sci.* **2023**, *11* (1), 173.

(6) Cai, Y. Y.; Yu, J.; Fu, G. F.; Li, H. Experimental investigation on the relevance of mechanical properties and porosity of sandstone after hydrochemical erosion. *J. Mt. Sci.* **2016**, *13* (11), 2053-2068.

(7) Yang, H.; Chen, C.; Ni, J.; Karekal, S. A hyperspectral evaluation approach for quantifying salt-induced weathering of sandstone. *Sci. Total Environ.* **2023**, *885*, 163886.

(8) Chen, C.; Yang, H.; Li, X.; Zhao, G.; Ni, J. Hyperspectral estimation method for deterioration of rock carvings in the humid regions of southern China. *Herit. Sci.* **2024**, *12* (1), 105.

(9) Sun, B.; Li, X. Y.; Cui, K.; Peng, N. B.; Hong, J.; Chen, R.; Jia, C. Study on the Characteristics of Damaged Sandstone in the Longshan Grottoes Using Water Chemistry and Freeze-Thaw Cycling. *Minerals* **2023**, *13* (3), 430.

(10) La Russa, M. F.; Comite, V.; Aly, N.; Barca, D.; Fermo, P.; Rovella, N.; Antonelli, F.; Tesser, E.; Aquino, M.; Ruffolo, S. A. Black crusts on Venetian built heritage, investigation on the impact of pollution sources on their composition. *The Eur. Phys. J. Plus* **2018**, *133* (9), 370.

(11) Morillas, H.; Maguregui, M.; Garcia-Florentino, C.; Carrero, J. A.; Salcedo, I.; Madariaga, J. M. The cauliflower-like black crusts on sandstones: A natural passive sampler to evaluate the surrounding environmental pollution. *Environ. Res.* **2016**, *147*, 218-232.

(12) Marszalek, M.; Alexandrowicz, Z.; Rzepa, G. Composition of weathering crusts on sandstones from natural outcrops and architectonic elements in an urban environment. *Environ. Sci. Pollut. Res.h* **2014**, *21* (24), 14023-14036.

(13) Zhang, Y.; Cao, C.; Du, H.; Huang, J.; Guo, X.; Luo, Q.; Ren, J. Investigation into the Gaseous SO2 Attack on Sandstone in the Yungang Grottoes. *Minerals* **2023**, *13* (1), 123.

(14) Zhang, J.; Li, Z.; Li, L.; Liu, J.; Liu, D.; Shao, M. Study on weathering mechanism of sandstone statues in Southwest China: example from the sandstone of Niche of Sakyamuni Entering Nirvana at Dazu Rock Carvings. *Nat. Hazards* **2021**, *108* (1), 775-797.

(15) Siegesmund, S.; Török, A.; Hüpers, A.; Müller, C.; Klemm, W. Mineralogical, geochemical and microfabric evidences of gypsum crusts: a case study from Budapest. *Environ. Geol.* **2006**, *52* (2), 385-397.

(16) Toniolo, L.; Zerbi, C. M.; Bugini, R. Black layers on historical architecture. *Environ. Sci. Pollut. Res.* **2008**, *16* (2), 218-226.

(17) Rovella, N.; Aly, N.; Comite, V.; Randazzo, L.; Fermo, P.; Barca, D.; Alvarez de Buergo, M.; La Russa, M. F. The environmental impact of air pollution on the built heritage of historic Cairo (Egypt). *Sci. Total Environ.* **2021**, *764*, 142905.

(18) De Kock, T.; Van Stappen, J.; Fronteau, G.; Boone, M.; De Boever, W.; Dagrain, F.; Silversmit, G.; Vincze, L.; Cnudde, V. Laminar gypsum crust on lede stone: Microspatial characterization and laboratory acid weathering. *Talanta* **2017**, *162*, 193-202.

(19) Islam, N.; Roy, K.; Barman, P.; Rabha, S.; Bora, H. K.; Khare, P.; Konwar, R.; Saikia, B. K. Chemical and toxicological studies on black crust formed over historical monuments as a probable health hazard. *J. Hazard. Mater.* **2024**, *464*, 132939.

(20) Matović, V.; Erić, S.; Kremenović, A.; Colomban, P.; Srećković-Batoćanin, D.; Matović, N. The origin of syngenite in black crusts on the limestone monument King's Gate (Belgrade Fortress, Serbia) – the role of agriculture fertiliser. *JgU. Cult. Herit.* **2012**, *13* (2), 175-186.

(21) Johnson, J. B.; Haneef, S. J.; Hepburn, B. J.; Hutchinson, A. J.; Thompson, G. E.; Wood, G. C. Laboratory exposure systems to simulate atmospheric degradation of building stone under dry and wet deposition conditions. *Atmos. Environ.* **1990**, *24* (10), 2585-2592.

(22) Feinberg, A.; Stenke, A.; Peter, T.; Hinckley, E.-L. S.; Driscoll, C. T.; Winkel, L. H. E. Reductions in the deposition of sulfur and selenium to agricultural soils pose risk of future nutrient deficiencies. *Commun. Earth Environ.* **2021**, *2* (1), 101.

(23) Senesi, G. S.; Carrara, I.; Nicolodelli, G.; Milori, D. M. B. P.; De Pascale, O. Laser cleaning and laser-induced breakdown spectroscopy applied in removing and characterizing black crusts from limestones of Castello Svevo, Bari, Italy: A case

study. *Microchem. J.* **2016**, *124*, 296-305.

(24) Barca, D.; Belfiore, C. M.; Crisci, G. M.; La Russa, M. F.; Pezzino, A.; Ruffolo, S. A. A new methodological approach for the chemical characterization of black crusts on building stones: a case study from the Catania city centre (Sicily, Italy). *J. Anal. At. Spectrom.* **2011**, *26* (5), 1000-1011.

(25) Bonazza, A.; Brimblecombe, P.; Grossi, C. M.; Sabbioni, C. Carbon in Black Crusts from the Tower of London. *Environ. Sci. Technol.* **2007**, *41* (12), 4199-4204.

(26) Marszałek, M. Application of Optical Microscopy and Scanning Electron Microscopy to the Study of Stone Weathering: A Cracow Case Study. *Int. J. Archit. Herit.* **2008**, *2* (1), 83-92.

(27) Wilhelm, K.; Longman, J.; Orr, S. A.; Viles, H. Stone-built heritage as a proxy archive for long-term historical air quality: A study of weathering crusts on three generations of stone sculptures on Broad Street, Oxford. *Sci. Total Environ.* **2021**, *759*, 143916.

(28) Wilhelm, K.; Longman, J.; Standish, C. D.; De Kock, T. The Historic Built Environment As a Long-Term Geochemical Archive: Telling the Time on the Urban "Pollution Clock". *Environ. Sci. Technol.* **2023**, *57* (33), 12362-12375.

(29) McKinley, J. M.; Curran, J. M.; Turkington, A. V. Gypsum formation in non-calcareous building sandstone: a case study of Scrabo sandstone. *Earth Surf. Processes Landf.* **2001**, *26* (8), 869-875.

(30) Veerle, C.; Geert, S.; Matthieu, B.; Jan, D.; Björn, D. S.; Tom, S.; Denis, V. L.; Yoni, D. W.; Marlina, E.; Laszlo, V.; et al. Multi-disciplinary characterisation of a

sandstone surface crust. *Sci. Total Environ.* **2009**, *407* (20), 5417-5427.

(31) Holynska, B.; Gilewicz-Wolter, J.; Ostachowicz, B.; Bielewski, M.; Streli, C.; Wobrauschek, P. Study of the deterioration of sandstone due to acid rain and humid SO2 gas. *X-Ray Spectrom.* **2004**, *33* (5), 342-348.

(32) Zhang, H.; Shi, M.; Shen, W.; Li, Z.; Zhang, B.; Liu, R.; Zhang, R. Damage or protection? The role of smoked crust on sandstones from Yungang Grottoes. *JAS* **2013**, *40* (2), 935-942.

(33) Liu, Z.; Zhu, L.; Zhang, B. In-situ formation of an aluminum phosphate coating with high calcite-lattice matching for the surface consolidation of limestone relics. *Constr. Build. Mater.* **2023**, *392*, 131836.

(34) UNESCO World Heritage Centre. World Heritage List. https://whc.unesco.org/en/list/912/ (UNESCO World Heritage Centre, Paris, 1999).

(35) Zhang, R. X.; Yang, S. Y. A Mathematical Model for Determining Carbon Coating Thickness and Its Application in Electron Probe Microanalysis. *Microsc. Microanal.* **2016**, *22* (6), 1374-1380.

(36) Yang, S. Y.; Jiang, S. Y.; Mao, Q.; Chen, Z. Y.; Rao, C.; Li, X. L.; Li, W. C.; Yang, W. Q.; He, P. L.; Li, X. Electron Probe Microanalysis in Geosciences: Analytical Procedures and Recent Advances. *At. Spectrosc.* **2022**, *43* (2), 186-200.

(37) B. Ravel and M. Newville, A., Artemis. Hephaestus: data analysis for X-ray absorption spectroscopy using IFEFFIT. *J. Synchrotron Radiat.* **2005**, 12, 537-541.

(38) Zeng, G. M.; Yu, Z.; Chen, Y. N.; Zhang, J. C.; Li, H.; Yu, M.; Zhao, M. J. Response

of compost maturity and microbial community composition to pentachlorophenol (PCP)-contaminated soil during composting. *Bioresour. Technol.* **2011**, *102* (10), 5905-5911.

(39) Chen, S. F.; Zhou, Y. Q.; Chen, Y. R.; Gu, J. fastp: an ultra-fast all-in-one FASTQ preprocessor. *Bioinformatics* **2018**, *34* (17), 884-890.

(40) Magoc, T.; Salzberg, S. L. FLASH: fast length adjustment of short reads to improve genome assemblies. *Bioinformatics* **2011**, *27* (21), 2957-2963.

(41) Edgar, R. C. UPARSE: highly accurate OTU sequences from microbial amplicon reads. *Nat. Methods* **2013**, *10* (10), 996-+.

(42) Sharma, A. K.; Vezzaro, L.; Birch, H.; Arnbjerg-Nielsen, K.; Mikkelsen, P. S. Effect of climate change on stormwater runoff characteristics and treatment efficiencies of stormwater retention ponds: a case study from Denmark using TSS and Cu as indicator pollutants. *SpringerPlus* **2016**, *5* (1).

(43) Cadar, E.; Sirbu, R.; Pirjol, B. S. N.; Ionescu, A. M.; Pirjol, T. N. Heavy Metals Bioaccumulation Capacity on Marine Algae Biomass from Romanian Black Sea Coast. *Rev. Chim.* **2019**, *70* (8), 3065-3072.

(44) González-Alcaraz, M. N.; van Gestel, C. A. M. Climate change effects on enchytraeid performance in metal-polluted soils explained from changes in metal bioavailability and bioaccumulation. *Environ. Res.* **2015**, *142*, 177-184.

(45) Di Benedetto, F.; D'Acapito, F.; Fornaciai, G.; Innocenti, M.; Montegrossi, G.; Pardi, L. A.; Tesi, S.; Romanelli, M. A Fe K-edge XAS study of amethyst. *Phys. Chem. Miner.* **2010**, *37* (5), 283-289.

(46) Muñoz, M.; Argoul, P.; Farges, F. Continuous Cauchy wavelet transform analyses of EXAFS spectra:: A qualitative approach. *Am. Mineral.* **2003**, *88* (4), 694-700.

(47) Carrero, J. A.; Arrizabalaga, I.; Bustamante, J.; Goienaga, N.; Arana, G.; Madariaga, J. M. Diagnosing the traffic impact on roadside soils through a multianalytical data analysis of the concentration profiles of traffic-related elements. *Sci. Total Environ.* **2013**, *458*, 427-434.

(48) Carrero, J. A.; Goienaga, N.; Olivares, M.; Martinez-Arkarazo, I.; Arana, G.; Madariaga, J. M. Raman spectroscopy assisted with XRF and chemical simulation to assess the synergic impacts of guardrails and traffic pollutants on urban soils. *J. Raman Spectrosc.* **2012**, *43* (10), 1498-1503.

(49) Lough, G. C.; Schauer, J. J.; Park, J. S.; Shafer, M. M.; Deminter, J. T.; Weinstein, J. P. Emissions of metals associated with motor vehicle roadways. *Environ. Sci. Technol.* **2005**, *39* (3), 826-836.

(50) Langner, P.; Mikutta, C.; Suess, E.; Marcus, M. A.; Kretzschmar, R. Spatial Distribution and Speciation of Arsenic in Peat Studied with Microfocused X-ray Fluorescence Spectrometry and X-ray Absorption Spectroscopy. *Environ. Sci. Technol.* **2013**, *47* (17), 9706-9714.

(51) Wade, A. M.; Richter, D. D.; Craft, C. B.; Bao, N. Y.; Heine, P. R.; Osteen, M. C.; Tan, K. G. Urban-Soil Pedogenesis Drives Contrasting Legacies of Lead from Paint and Gasoline in City Soil. *Environ. Sci. Technol.* **2021**, *55* (12), 7981-7989.

(52) Chien, C. T.; Benahabet, T.; Torfstein, A.; Paytan, A. Contributions of Atmospheric Deposition to Pb Concentration and Isotopic Composition in Seawater and

Particulate Matters in the Gulf of Aqaba, Red Sea. *Environ. Sci. Technol.* **2019**, *53* (11), 6162-6170.

(53) Wan, D. J.; Yang, H. D.; Jin, Z. D.; Xue, B.; Song, L.; Mao, X.; Yang, J. S. Spatiotemporal trends of atmospheric Pb over the last century across inland China. *Sci. Total Environ.* **2020**, *729*, 138399.

(54) Pey, J.; Pérez, N.; Cortés, J.; Alastuey, A.; Querol, X. Chemical fingerprint and impact of shipping emissions over a western Mediterranean metropolis: Primary and aged contributions. *Sci. Total Environ.* **2013**, *463*, 497-507.

(55) Yu, B. Y.; Zhao, G. P.; An, R. Y. Framing the picture of energy consumption in China. *Nat. Hazards* **2019**, *99* (3), 1469-1490.

(56) Pant, P.; Harrison, R. M. Estimation of the contribution of road traffic emissions to particulate matter concentrations from field measurements: A review. *Atmos. Environ.* **2013**, *77*, 78-97.

(57) Sanjurjo-Sánchez, J.; Alves, C.; Freire-Lista, D. M. Biomineral deposits and coatings on stone monuments as biodeterioration fingerprints. *Sci. Total Environ.* **2024**, *912*, 168846.

(58) Metelka, V.; Baratoux, L.; Jessell, M. W.; Naba, S. Visible and infrared properties of unaltered to weathered rocks from Precambrian granite-greenstone terrains of the West African Craton. *J. Afr. Earth Sci.* **2015**, *112*, 570-585.

(59) Yang, H.; Ni, J.; Chen, C.; Chen, Y. Weathering assessment approach for building sandstone using hyperspectral imaging technique. *Herit. Sci.* **2023**, *11* (1), 70.

(60) Wang, T.; Liu, Y. Y.; Deng, Y.; Fu, H. B.; Zhang, L. W.; Chen, J. M. Adsorption of

SO2 on mineral dust particles influenced by atmospheric moisture. *Atmos. Environ.* **2018**, *191*, 153-161.

(61) Zhang, T.; Zhang, H. J. Microbial Consortia Are Needed to Degrade Soil Pollutants. *Microorganisms* **2022**, *10* (2), 261.

(62) He, J.; Zhang, N.; Shen, X.; Muhammad, A.; Shao, Y. Deciphering environmental resistome and mobilome risks on the stone monument: A reservoir of antimicrobial resistance genes. *Sci. Total Environ.* **2022**, *838*, 156443.

(63) Saadouli, I.; Marasco, R.; Mejri, L.; Hamden, H.; Guerfali, M. M. s.; Stathopoulou, P.; Daffonchio, D.; Cherif, A.; Ouzari, H.-I.; Tsiamis, G.; et al. Diversity and adaptation properties of actinobacteria associated with Tunisian stone ruins. *Front. Microbiol.* **2022**, *13*, 997832.

(64) Cappitelli, F.; Toniolo, L.; Sansonetti, A.; Gulotta, D.; Ranalli, G.; Zanardini, E.; Sorlini, C. Advantages of using microbial technology in removal of black technology over traditional chemical crusts from stone surfaces of historical monuments. *Appl. Environ. Microbiol.* **2007**, *73* (17), 5671-5675.

(65) Guan, X.; Yuan, X. Z.; Zhao, Y. L.; Bai, J.; Li, Y.; Cao, Y. X.; Chen, Y.; Xiong, T. Adsorption behaviors and mechanisms of Fe/Mg layered double hydroxide loaded on bentonite on Cd (II) and Pb (II) removal. *J. Colloid Interface Sci.* **2022**, *612*, 572-583.

(66) Jiang, M.; Wang, K.; Li, G.; Zhao, Q. L.; Wang, W. Y.; Jiang, J. Q.; Wang, Y. P.; Yuan, L. Z. Stabilization of arsenic, antimony, and lead in contaminated soil with montmorillonite modified by ferrihydrite: Efficiency and mechanism. *Chem. Eng.*

J. **2023**, *457*.

(67) Zhu, R. L.; Chen, Q. Z.; Zhou, Q.; Xi, Y. F.; Zhu, J. X.; He, H. P. Adsorbents based on montmorillonite for contaminant removal from water: A review. *Appl. Clay Sci.* **2016**, *123*, 239-258.

(68) Bhattacharyya, K. G.; Gupta, S. S. Adsorption of a few heavy metals on natural and modified kaolinite and montmorillonite: A review. *Adv. Colloid Interface Sci.* **2008**, *140* (2), 114-131.

(69) O'Day, P. A.; Vlassopoulos, D. Mineral-Based Amendments for Remediation. *Elements* **2010**, *6* (6), 375-381.

(70) Scheidegger, A. M.; Lamble, G. M.; Sparks, D. L. Spectroscopic Evidence for the Formation of Mixed-Cation Hydroxide Phases upon Metal Sorption on Clays and Aluminum Oxides. *J. Colloid Interface Sci.* **1997**, *186* (1), 118-128.

(71) Parvizpour, S.; Jamshidi, A.; Sarikhani, R.; Dehnavi, A. G. The pH effect of sulfuric acid on the physico-mechanical properties of Atashkuh travertine, Central Iran. *Environ. Earth Sci.* **2022**, *81* (5), 159.

(72) Zhao, S. P.; He, J. J.; Dong, L. X.; Qi, S. F.; Yin, D. Y.; Chen, J. B.; Yu, Y. Contrasting Vertical Circulation between Severe and Light Air Pollution inside a Deep Basin Results from the Collaborative Experiment of 3D Boundary-Layer Meteorology and Pollution at the Sichuan Basin (BLMP-SCB). *Bull. Am. Meteorol. Soc.* **2023**, *104* (2), E411-E434.